Angewandte Chemie

Selective inhibitors of FKBP51 employ conformational selection of dynamic invisible states

--Manuscript Draft--

Manuscript Number:	
Article Type:	Communication
Corresponding Author:	Michael Sattler Technische Universitat Munchen Garching, GERMANY
Corresponding Author E-Mail:	sattler@helmholtz-muenchen.de
Order of Authors (with Contributor Roles):	Pravin Kumar Ankush Jagtap
	Sam Asami
	Claudia Sippel
	Ville Kaila
	Felix Hausch
	Michael Sattler
Keywords:	Drug selectivity; protein dynamics; NMR; conformational selection; FKBP51
Manuscript Classifications:	Drug design; Inhibitors; Molecular dynamics; NMR spectroscopy; Structural Biology
Suggested Reviewers:	Wolfgang Jahnke Novartis wolfgang.jahnke@novartis.com NMR, drug discovery
	Christian Griesinger MPI Goettingen cigr@nmr.mpibpc.mpg.de NMR methods, dynamics, drug discovery
	Stephen Fesik U Vanderbilt, USA stephen.fesik@vanderbilt.edu NMR, drug discovery
	Malcolm Walkinshaw The University of Edinburgh M.walkinshaw@ed.ac.uk Structural biologist with track record in immunophilin drug discovery
	Guy Lippens Bibliotheque de l'INSA de Toulouse glippens@insa-toulouse.fr NMR structural biologist, worked on FKBP proteins
	Mikael Akke Lunds Universitet Mikael.Akke@bpc.lu.se NMR, protein dynamics
Opposed Reviewers:	Teresa Carlomagno Leibniz Universitat Hannover teresa.carlomagno@oci.uni-hannover.de competing interests
	David LeMaster University at Albany, SUNY david.lemaster@health.ny.gov competing interests

	Griselda Hernandez University at Albany, SUNY griselda.hernandez@health.ny.gov competing interests
Abstract:	Targeting conserved ligand binding pockets in homologous proteins with selective inhibitors presents a difficult challenge in drug discovery. The recently discovered SAFit class inhibitors against the Hsp90 co-chaperone FKBP51 show >10,000--fold selectivity over its closely related paralog FKBP52, demonstrating that excellent selectivity within highly conserved protein families is possible. However, the mechanism underlying this selectivity remained unknown. Here, by combining NMR, biophysical and computational methods with mutational analysis, we unravel the binding mechanism of the SAFit inhibitors to FKBP51. We show that the SAFit molecules bind to a transient pocket that represents a weakly populated conformation resembling the inhibitor-bound state of FKBP51, suggesting conformational selection and not induced fit as major binding mechanism. The inhibitor-bound conformation of FKBP51 is stabilized by an allosteric network of residues located away from the inhibitor-binding site. Theses residues stabilize the Phe67 side chain in a dynamic outward conformation and are distinct in FKBP52, thus rationalizing the basis for the selectivity of SAFit inhibitors. Our results represent a paradigm highlighting principles for the selective inhibition of transient binding pockets.
Author Comments:	Dear Dr. Compton, We submit the following manuscript for your consideration for publication as a Communication in Angewandte Chemie: Selective inhibitors of FKBP51 employ conformational selection of dynamic invisible states by Pravin Kumar Ankush Jagtap, Sam Asami, Claudia Sippel, Ville R. I. Kaila, Felix Hausch, and Michael Sattler Selectively targeting conserved ligand binding pockets in homologous proteins with isoform-selective inhibitors presents a difficult challenge in drug discovery, but is essential to develop specific and safe drugs. Some of us have recently developed isoform-specific SAFit class of inhibitors against the Hsp90 co-chaperone FKBP51 with >10,000--fold selectivity over its closely related paralog FKBP52. Differences in free and ligand bound crystal structures might suggest an induced fit binding mechanism. However, given that the binding pocket for the ligand is not accessible in the unbound form suggests a more complex binding mechanism that must involve an essential role for conformational dynamics. Thus, the molecular mechanisms that explain the unique selectivity of SAFit inhibitors remained unknown. As the mechanistic principles underlying this selectivity are expected to represent a general paradigm that could be utilized for the development of selective inhibitors in other systems, we studied these in the current manuscript. Here, we combine NMR, biophysical and computational methods (molecular dynamics, quantum chemical calculations) with mutational analysis to unravel the binding mechanism of selective FKBP51 inhibitors. Key findings of our manuscript are: •Access to the ligand binding pocket of FBKP51 is gated by the aromatic side chain of Phe67. We show that this side chain dynamically samples inward and outward conformations using NMR relaxation dispersion experiments. •We provide evidence that FKBP51-selective SAFit inhibitors bind to a dynamic, weakly populated binding pocket that is sampled <1% of existing conformations in solution resembling the inhibitor-bound state of FKBP51. •Our findings suggests a key role for conformational selection and not induced fit as major binding mechanism. •The inhibitor-bound conformation of FKBP51 is stabilized by an allosteric network of residues located away from the inhibitor-binding site. These residues stabilize the Phe67 side chain in a dynamic outward conformation and are distinct in FKBP52, thus rationalizing the basis for the selectivity of SAFit inhibitors.

	Our results represent a paradigm highlighting principles for the selective inhibition of transient binding pockets. We believe that this manuscript is of interest to a broad audience of Angewandte especially in the fields of drug discovery, medicinal chemistry and structural biology. This manuscript has not been published and is not under consideration for publication elsewhere. We have no conflicts of interest to disclose. Please find below a suggestion for potential reviewers. Thank you for your consideration! We are looking forward to hearing from you. Sincerely, Michael Sattler
Section/Category:	
Additional Information:	
Question	**Response**
Submitted solely to this journal?	Yes
Has there been a previous version?	No
Do you or any of your co-authors have a conflict of interest to declare?	No. The authors declare no conflict of interest.

WILEY-VCH

COMMUNICATION

Selective inhibitors of FKBP51 employ conformational selection of dynamic invisible states

Pravin Kumar Ankush Jagtap,[+] Sam Asami,[+] Claudia Sippel, Ville R. I. Kaila, Felix Hausch, and Michael Sattler*

Abstract: Targeting conserved ligand binding pockets in homologous proteins with selective inhibitors presents a difficult challenge in drug discovery. The recently discovered SAFit class inhibitors against the Hsp90 co-chaperone FKBP51 show >10,000⁻fold selectivity over its closely related paralog FKBP52, demonstrating that excellent selectivity within highly conserved protein families is possible. However, the mechanism underlying this selectivity remained unknown. Here, by combining NMR, biophysical and computational methods with mutational analysis, we unravel the binding mechanism of the SAFit inhibitors to FKBP51. We show that the SAFit molecules bind to a transient pocket that represents a weakly populated conformation resembling the inhibitor-bound state of FKBP51, suggesting conformational selection and not induced fit as major binding mechanism. The inhibitor-bound conformation of FKBP51 is stabilized by an allosteric network of residues located away from the inhibitor-binding site. Theses residues stabilize the Phe67 side chain in a dynamic outward conformation and are distinct in FKBP52, thus rationalizing the basis for the selectivity of SAFit inhibitors. Our results represent a paradigm highlighting principles for the selective inhibition of transient binding pockets.

Protein dynamics plays a crucial role in ligand binding[1]. However rational drug design is generally focused on targeting low energy conformations observed in static protein structures[2], while the conformational dynamics of the binding surface is usually neglected during this process. Notably, exploiting differential conformational dynamics could provide a unique strategy to design selective inhibitors against homologous proteins, where selective targeting of highly conserved active sites is challenging. Targeting dynamic regions involving less conserved residues thus offers an attractive strategy to selectively inhibit homologous proteins.

FK506 binding protein 51 (FKBP51) is a co-chaperone of the heat shock protein Hsp90 and is best known for its regulation of steroid hormone receptor responsiveness[3]. Notably, the regulation of glucocorticoid hormone receptor activity by FKBP51 is antagonized by its close paralog FKBP52, where FKBP51 inhibits and FKBP52 enhances glucocorticoid receptor activity, respectively. Inhibition of FKBP51 has been suggested as a novel treatment option for stress related disorders[3b, 4], obesity[5] and chronic pain[6]. However, discrimination against FKBP52 is thought to be critical due to the counteracting roles of FKBP51/52, e.g., in development, stress-coping behavior, stress hormone signaling and metabolism. Prior to the recent discovery of the SAFit class of inhibitors such as SAFit1 and iFit4 (**Figure S1**) that selectively target FKBP51[7], the distinct roles of FKBP51/52 could not be pharmacologically delineated due to their highly conserved binding pockets. NMR[8] and MD[9] studies indicated the presence of protein dynamics at nanosecond timescales in FKBP51. Moreover, mutational analysis revealed that the Lys58, Lys60 and Phe129 in FKBP51, which are distinct from FBKP52 and are located remote from the SAFit binding site, are responsible for the selectivity[7a]. However, the underlying molecular mechanism for the selective SAFit binding to FKBP51 remains unknown.

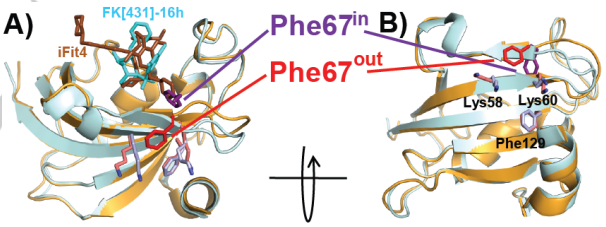

Figure 1. A) Structural superposition of the FK506-binding domain of FKBP51 in complex with FK[431]-16h (light cyan, PDB ID: 5OBK) and the SAFit analog iFit4 (light orange, PDB ID: 4TW7). FK[431]-16h and iFit4 are shown in cyan and brown sticks. The two conformations of Phe67 (Phe67^{in} and Phe67^{out}) observed in FKBP51+FK[431]-16h and FKBP51+iFit4 complex structures, respectively, are highlighted as purple and red sticks. B) Side view of A) with the ligands omitted for clarity. The residues which stabilize Phe67^{out} (Lys58, Lys60 and Phe129) are shown as light blue and orange sticks for the FK[431]-16h and iFit4 complexes, respectively.

The crystal structure of the ligand binding FK1 domain of FKBP51 (called FKBP51^{WT} hereafter) bound to various SAFit derivatives indicates[7] that the side chain of Phe67, which is displaced to accommodate the cyclohexyl moiety of SAFit1, is stabilized by the side chains of Lys58 and Lys60 and indirectly by Phe129 in the outward conformation (**Figure 1**). FKBP52 exhibits distinct amino acids in these positions (Thr58, Trp60, and Val129). A swap of these residues between FKBP51 and 52 leads to a complete reversal of selectivity for SAFit ligands[7a]. As there are only minor differences in the side chain conformations of FKBP51 between the free and the SAFit-bound crystal structures except for the side-chain conformations of Lys58, Lys60 and Phe67, we

Dr. P.K.A. Jagtap,[+] Dr. S. Asami,[+] Prof. Dr. M.Sattler
Lehrstuhl für Biomolekulare NMR-Spektroskopie
Technische Universität München
Lichtenbergstr. 4, 85747 Garching (Germany)
E-mail: michael.sattler@tum.de, sattler@helmholtz-muenchen.de

C. Sippel, Prof. Dr. F. Hausch
Max Planck Institute of Psychiatry
Kraepelinstr. 2–10, 80804 Munich (Germany)

Present address: Prof. Dr. F. Hausch
Structure-Based Drug Research
Technisch Universität Darmstadt
Alarich-Weiss-Str. 4, 64287 Darmstadt (Germany)

Prof. Dr. V.R.I. Kaila
Department Chemie
Technische Universität München
Lichtenbergstr. 4, 85747 Garching (Germany)

[+] These two authors made equal contribution to this paper.

Supporting information for this article is given via a link at the end of the document.

hypothesize here that conformational dynamics of these and surrounding residues could provide clues for the selectivity of SAFit-type inhibitors for FKBP51. NMR ^{15}N relaxation data indicate that the unbound FK1 domain exhibits significant internal motion[8b, 10], but it remains unclear how this relates to the selective inhibition of FKBP51. In order to quantitatively measure internal motion at ps-ns and μs-ms time scales we recorded ^{15}N backbone NMR autorelaxation[11] and relaxation dispersion experiments[12], respectively for the free and SAFit1-bound FKBP51 FK1 domain (**Figure S2 and S4**).

An analysis of the ^{15}N transverse relaxation data in FKBP51^{WT} indicates substantially increased R_2 relaxation rates in the presence of the selective inhibitor SAFit1 as compared to unbound FKBP51^{WT} **(Figure S2B)**. These increased R_2 rates are most prominent for residues in the β_{3a} strand, which contains Phe67 (**Figure S2E**). Moreover, when bound to SAFit1, the amide NMR resonances of Lys58 to Ser62 in the β_2 strand and the β_{3a}-β_{3b} loop are broadened beyond detection (**Figure S3**). This suggests that SAFit1 binding induces a gain of motion in the μs-ms time scale. Such increased dynamics is unexpected as inhibitor binding usually rigidifies and thus suppresses conformational dynamics in proteins. Indeed, binding of the canonical inhibitor compound FK[431]-16h[13] (**Figure S1**), a bicyclic analogue of FK506, that does not induce the iFit-typical conformational change in FKBP51 and binds with similar affinity to FKBP52[14], is associated with the expected loss of motion (**Figure S2**). This demonstrates that the unusual gain of motion is a unique feature of SAFit binding.

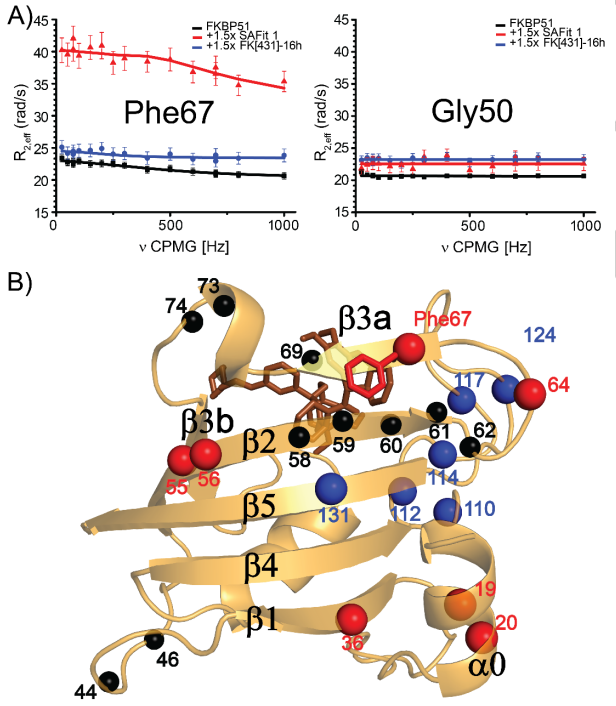

Figure 2. Relaxation dispersion experiments of FKBP51^{WT} free and bound to SAFit1 or FK[431]-16h ligands. A) ^{15}N backbone relaxation dispersion curves of Phe67 and Gly50. Phe67 shows minor dispersion in FKBP51^{WT}, but significantly increased dynamics upon SAFit1 binding. For comparison, Gly50 does not show dispersion in ligand free and bound states. B) Backbone amides of residues, which show gain (red spheres) or loss (blue spheres) of motion (with $\Delta R_{ex} \geq 2$ rad/s) upon SAFit1 binding relative to FKBP^{WT} are shown with the crystal structure of the FKBP51^{WT}+iFit4 complex (PDB ID: 4TW7). The ligand and the Phe67 side chain are shown in orange and red sticks, respectively. Black spheres represent residues that are line-broadened beyond detection.

To characterize the change in dynamics at μs-ms timescale upon SAFit1 binding to FKBP51 and to probe if FKBP51^{WT} samples the SAFit1 bound state even in the absence of ligand, we performed ^{15}N CPMG relaxation dispersion experiments[12b, 15] on FKBP51^{WT}, FKBP51^{WT}+SAFit1 and FKBP51^{WT}+FK[431]-16h (**Figure 2, S4**). Intriguingly, these experiments show that while binding of the canonical inhibitor FK[431]-16h almost completely abolishes internal motion at μs-ms timescales, binding of the selective inhibitor SAFit1 leads to a redistribution of μs-ms motion within the protein. The relaxation dispersion data in the absence of inhibitors indicate that residues, which experience motion at μs-ms timescales, mainly affect the β_4-β_5 loop and that internal dynamics is also seen for residues near Phe67 (**Figure S4)**.

Figure 2A shows the relaxation dispersion profile for Phe67 in the apo and SAFit1-bound state, respectively, for which clear conformational exchange is observed in the unbound state. When fitting the CPMG data for all residues in the β3a strand simultaneously and assuming a 2-site exchange, we obtain a minor state population of 0.34% and an absolute chemical shift difference, $|\Delta\omega_{CPMG}(^{15}N)|$, between the minor and the major state of 4.38 ppm (**Supplementary Table 1**). In order to validate the origin of this large chemical shift difference, we performed atomistic 100 ns molecular dynamics (MD) simulations of apo- and SAFit-bound FKBP51. The chemical shielding of Phe67 using was estimated using quantum chemical density functional theory (DFT) calculations based on the MD-relaxed structures (**Supplementary Material**). During the MD simulations, Phe67 remains in the outward conformation of the SAFit-bound structure, whereas in the apo-form, Phe67 turns towards the protein framework, leading to conformational changes in the backbone contacts (**Figure S6**). We also find that removal of the ligand from the SAFit-bound simulations, perturbs the Phe67 conformation towards the *apo*-bound form. Interestingly, the DFT calculations suggest that these conformational changes lead to a ^{15}N chemical shift difference for the backbone nitrogen of Phe67 of ≈ +4-7 ppm by DFT, which compares well to the chemical shift difference of +4.52 ppm extracted from HSQC spectra of free and bound FKBP51^{WT} (**Figure S5**) as well as to the CPMG-derived absolute chemical shift difference of 4.4 ppm. This chemical shift difference likely reflects changes in the electronic structure when the backbone N-H of Phe67 is in contact with protein backbone or bulk solvent water (**Figure S6C**). The DFT and experimental chemical shifts thus support the notion that the CPMG-identified minor conformation corresponds to an apo-Phe^{out}–like state, seen in the FKBP51-iFit4 complex, thus indicating conformational selection as binding mechanism.

In the SAFit1-bound form the pattern of residues showing slow exchange dynamics is largely different compared to the unbound protein. Conformational exchange in the loop connecting β_4 and β_5 is suppressed, possibly due to multiple interactions and stabilization of this loop with the ligand. However, Phe67 shows a significant enhancement of μs-ms motion in the presence of SAFit1 along with several residues spread throughout the protein (**Figure 2; Figure S2**). Interestingly, the conformational flexibility gained in the presence of SAFit1 is most prominent for helix α_0, which is most distal from the ligand-binding site (**Figure 2B**). This suggests, that the conformational dynamics in the ligand-binding site is coupled allosterically via Phe67 to the distal α_0 helix by a

collective movement of amino acids in the β_{3a}, β_2, β_5, β_4 and β_1 strands. Moreover, most of the residues, which exhibit increased dynamics upon SAFit1 binding, are located remote from the ligand-binding interface, further supporting this notion (**Figure S4**). This is in contrast to the strong reduction of conformational dynamics observed in the FK[431]-16h-bound state, where addition of ligand quenches protein dynamics for almost all residues.

As NMR relaxation dispersion experiments on FKBP51^{WT} suggest the presence of a minor apo-Phe67^{out} state and considering that we observe increased line broadening in the presence of SAFit1, we hypothesized that this broadening is linked to the Phe67 outward conformation. To test this, we designed the FKBP51^{Phe67Tyr} mutant, where Tyr67 is expected to more often sample the outward conformation in the apo form relative to the wildtype protein, as the para-hydroxyl group of tyrosine may cause steric clashes in the inward conformation. Consistent with this hypothesis, the ^{1}H,^{15}N HSQC spectrum of FKBP51^{Phe67Tyr} shows severe line broadening of residues at the tip of the β_2 strand, especially for amide signals of Gly59, Lys60 and Phe129 in strand β_5 (**Figure S7A**). This pattern of line broadening is similar to that observed in FKBP51^{WT}+SAFit1 (**Figure S7C**) suggesting that the line broadening observed for residues in β_{3a} and β_2 of the FKBP51^{Phe67Tyr} mutant is linked to conformational dynamics associated with an outward conformation of Tyr67.

As all canonical FKBP51 inhibitors studied so far unequivocally bind to FKBP51 with an inward conformation of Phe67[14, 16] , we sought to stabilize the inward conformation of Tyr67 by titrating FKBP51^{Phe67Tyr} with compound FK[431]-16h. This leads to a significant reduction of line broadening (**Figure S8**) for Gly59, Lys60 and Phe129 amide signals in the ^{1}H, ^{15}N HSQC spectrum of FKBP51^{Phe67Tyr}+compound FK[431]-16h. Amide NMR signals of these residues are also detected for the unbound FKBP51^{WT} (**Figure S3A**), which adopts the inward conformation in the crystal structure. Therefore, line broadening of amide signals from the tip of β_2 strand (Gly59 and Lys60) and of Phe129 reports on the conformation of Phe67 and represents a signature of the conformational state of the Phe67 side chain. Notably, Lys58, Lys60 (both neighbours to Gly59) and Phe129 are the residues that have been shown to confer selectivity for SAFit1 binding.

Table 1. ITC-derived thermodynamic parameters for inhibitor binding to FKBP51 wildtype and mutants

Sample[a]	K_D (nM)	ΔH (kcal/mol)	-TΔS (kcal/mol)	ΔG (kcal/mol)
FKBP51^{WT} +SAFit1	40.4±9.3	-7.2±0.07	-2.9±0.34	-10.1±0.35
FKBP51^{Phe67Tyr} +SAFit1	9.2±2.7	-11.9±0.07	0.9±0.04	-11.1±0.41
FKBP51^{Phe67Val} +SAFit1	14.7±2.7	-11.7±0.05	1.0±0.07	-10.7 ±0.91
FKBP51^{WT} +FK[431]-16h	148.9±17.1	-12.5±0.11	3.2±0.10	-9.3±0.15
FKBP51^{Phe67Tyr} +FK[431]-16h	636.2±67.8	-8.4±0.13	-0.1±0.03	-8.5±0.1
FKBP51^{Phe67Val} +FK[431]-16h	76.0±8.7	-11.0±0.04	1.3±0.08	-9.8±0.90

[a] Errors calculated from two independent measurements.

The outward conformation of the Phe67 sidechain in SAFit1-bound FKBP51^{WT} exposes the aromatic sidechain from a hydrophobic to a hydrophilic solvent environment. This is expected to be associated with an energetic penalty. In order to test if the shape and hydrophobicity of the residue at position 67 affects inhibitor binding to FKBP51, we studied the FKBP51^{Phe67Val} mutant. The smaller valine side chain and its lower desolvation energy compared to phenylalanine[17] might thermodynamically favour the inward state. Thus, Val67 in the FKBP51^{Phe67Val} mutant is expected to prefer the inward conformation in the absence of SAFit1, similar to FKBP51^{WT} and stabilize the outward state in the presence of SAFit1 in comparison to FKBP51^{WT}. Indeed, in the FKBP51^{Phe67Val} mutant the signature amide NMR signals of Gly59, Lys60 and Phe129 do not exhibit line broadening, consistent with the inward conformation of Val67 in this mutant in the absence of SAFit1 (**Figure S7 B,C**).

To characterize the thermodynamic features of SAFit-type binding we performed ITC experiments with wildtype and mutant FKBP51 proteins (**Table 1**). We expected a stronger interaction of SAFit1 with both mutants: an outward conformation of Tyr67 in FKBP51^{Phe67Tyr} should increase the population of a preformed binding pocket in the apo state without requiring a major conformational rearrangement. Binding of SAFit1 to the FKBP51^{Phe67Val} mutant should also be more favourable as compared to FKBP51^{WT} due to reduced enthalpic penalty for displacing the smaller Val67 sidechain from the binding pocket to accommodate the cyclohexyl moiety of SAFit1. Indeed, both mutants show a 4-fold increase in affinity for SAFit1 relative to FKBP51^{WT}. The increased affinity is associated with a ∼1.6 fold increase in binding enthalpy likely due to tighter interaction of SAFit1 with the mutants (**Supplementary discussion**). The canonical inhibitor FK[431]-16h shows a modest 2-fold increase in affinity for FKBP^{Phe67Val} binding presumably due to extra space in the binding pocket and a 4-fold decrease in binding affinity for FKBP^{Phe67Tyr} binding likely due to steric clashes in the binding pocket of the additional para-hydroxyl group of Tyr67.

To assess the kinetic features of SAFit1 binding to FKBP51^{WT}, FKBP51^{Phe67Tyr} and FKBP51^{Phe67Val} mutants, we determined the kinetic binding rates by surface plasmon resonance (SPR) (**Table 2**, **Table S2**, **Figure S9**).

Table 2. SPR parameters for ligand binding to FKBP51^{WT} and mutants.

Sample	k_{on} (x10^5) (1/Ms)[a]	k_{off} (x10^{-2}) (1/s) [a]
FKBP51^{WT}+SAFit1	1.17 ± 0.02	2.13 ± 0.04
FKBP51^{Phe67Tyr}+SAFit1	7.96 ± 0.46	2.68 ± 0.16
FKBP51^{Phe67Val}+SAFit1	1.53 ± 0.02	0.98 ± 0.01
FKBP51^{WT}+FK[431]-16h	3.40 ± 0.04	1.49 ± 0.01
FKBP51^{Phe67Tyr}+FK[431]-16h	1.83 ± 0.03	n.d.
FKBP51^{Phe67Val}+FK[431]-16h	5.78 ± 0.14	3.2 ± 0.08

[a] Errors represent standard error of fitting. n.d.: not determined

FKBP51^{Phe67Tyr} shows a ≈7 -fold faster association rate k_{on} for SAFit1 binding with no significant change in k_{off} rates compared to the wildtype protein. (**Figure 3**), consistent with an increased population of the outward conformation of Tyr67. On the other hand, the increase in affinity of SAFit1 for FKBP^{Phe67Val} appears mainly driven by the slower k_{off} rate (2.2-fold) with only a minor increase in the k_{on} rate (1.3 fold), consistent with valine being more stable in a solvent-exposed environment than the bulky aromatic side chains as discussed above. As the hydrophobicity of the residue at position 67 in FKBP51 modulates the off-rate for SAFit1 binding, the stability of the outward

conformation of Phe67^{out} in the FKBP51^{WT} in the solvent environment seems a crucial factor governing the SAFit1 affinity.

In conclusion, our NMR experiments show that a minor population of FKBP51 pre-exists in a dynamic equilibrium with the Phe67^{out} conformation, which is conformationally selected upon binding to SAFit1. Considering that the overall binding affinity is governed by both k_{on} and k_{off} rates, stabilizing Phe67 in the solvent-exposed environment outward conformation appears important. Dynamic interactions with residues Lys58, Lys60 and Phe129 stabilize the Phe67^{out} conformation in FKBP51^{WT}+SAFit1. This is consistent with and rationalizes the residue-swap mutations in FKBP51 and 52 that lead to a reversal of selectivity [7a]. This concerted conformational motion at µs-ms timescales is supported by the line broadening upon SAFit1 binding indicated by our NMR experiments.

Ligand dissociation rates have been previously correlated with protein dynamics[1b]. Minor variations of homologous proteins even remote from the ligand-binding site could significantly affect the k_{off} rates and thus the selectivity of the ligand binding by directly modulating the protein dynamics. Our results show that understanding protein dynamics provides crucial clues for the design of new selective inhibitors.

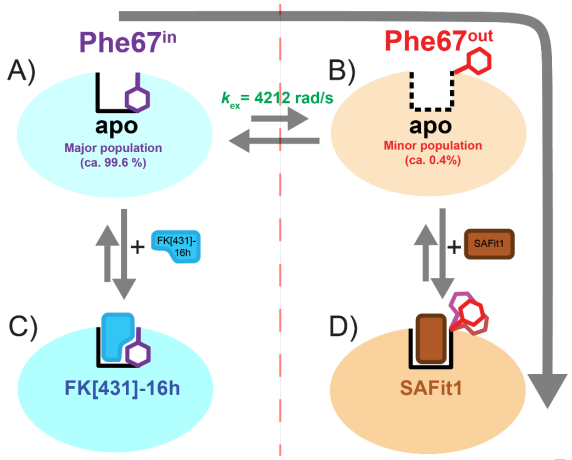

Figure 3. Binding mechanisms for the interaction of FK506-binding domain of FKBP51 with selective and non-selective ligands. (A) Phe67 adopts an inward orientation in the crystal structure of apo-Phe67^{in}. (B) NMR data show that this conformation is in a dynamic equilibrium (k_{ex} = k_1 + k_{-1} = 4212 rad/s) with a weakly populated apo-Phe67^{out} state. (C) The non-selective FK506 analogue FK[431]-16h binds to the apo-Phe67^{in} state. (D) The selective ligand iFit4/SAfit1 binds to the minor pre-existing population of apo-Phe67^{out} detected by NMR.

Acknowledgements

This work was supported by the DFG grants SFB1035 (to M.S. and V.K.) and GRK1721 (to M.S.), EU HORIZON 2020 ITN AEGIS, (to M.S), the M4 Award 2015 (BIO-1601-0003 to FH) and the BMBF/ERA-IB grant 'TACRODRUGS' (031B0269B to FH). PKAJ acknowledges a doctoral fellowship from the Boehringer Ingelheim Fonds.

Keywords: Protein dynamics • NMR • conformational selection • drug selectivity • FKBP51 • conformational entropy

[1] a) M. H. Seo, J. Park, E. Kim, S. Hohng, H. S. Kim, *Nat Commun* **2014**, *5*, 3724; b) M. J. Carroll, R. V. Mauldin, A. V. Gromova, S. F. Singleton, E. J. Collins, A. L. Lee, *Nat. Chem. Biol.* **2012**, *8*, 246-252; c) D. D. Boehr, R. Nussinov, P. E. Wright, *Nat. Chem. Biol.* **2009**, *5*, 789-796.

[2] a) A. Stank, D. B. Kokh, J. C. Fuller, R. C. Wade, *Acc Chem Res* **2016**, *49*, 809-815; b) V. Oleinikovas, G. Saladino, B. P. Cossins, F. L. Gervasio, *J. Am. Chem. Soc.* **2016**, *138*, 14257-14263; c) S. Muller, A. Chaikuad, N. S. Gray, S. Knapp, *Nat. Chem. Biol.* **2015**, *11*, 818-821; d) V. S. Shaw, H. Mohammadiarani, H. Vashisth, R. R. Neubig, *J. Am. Chem. Soc.* **2018**, *140*, 3454-3460; e) R. F. Ludlow, M. L. Verdonk, H. K. Saini, I. J. Tickle, H. Jhoti, *Proc Natl Acad Sci U S A* **2015**, *112*, 15910-15915; f) S. Eyrisch, V. Helms, *J. Med. Chem.* **2007**, *50*, 3457-3464; g) C. Rechlin, F. Scheer, F. Terwesten, T. Wulsdorf, E. Pol, V. Fridh, P. Toth, W. E. Diederich, A. Heine, G. Klebe, *ACS Chem Biol* **2017**, *12*, 1397-1415; h) S. Boulton, G. Melacini, *Chem Rev* **2016**, *116*, 6267-6304; i) H. Kubinyi, *Current opinion in drug discovery & development* **1998**, *1*, 4-15.

[3] a) D. L. Cioffi, T. R. Hubler, J. G. Scammell, *Curr Opin Pharmacol* **2011**, *11*, 308-313; b) M. V. Schmidt, M. Paez-Pereda, F. Holsboer, F. Hausch, *ChemMedChem* **2012**, *7*, 1351-1359.

[4] a) J. Hartmann, K. V. Wagner, C. Liebl, S. H. Scharf, X. D. Wang, M. Wolf, F. Hausch, T. Rein, U. Schmidt, C. Touma, J. Cheung-Flynn, M. B. Cox, D. F. Smith, F. Holsboer, M. B. Muller, M. V. Schmidt, *Neuropharmacology* **2012**, *62*, 332-339; b) J. C. O'Leary, 3rd, S. Dharia, L. J. Blair, S. Brady, A. G. Johnson, M. Peters, J. Cheung-Flynn, M. B. Cox, G. de Erausquin, E. J. Weeber, U. K. Jinwal, C. A. Dickey, *PloS one* **2011**, *6*, e24840; c) C. Touma, N. C. Gassen, L. Herrmann, J. Cheung-Flynn, D. R. Bull, I. A. Ionescu, J. M. Heinzmann, A. Knapman, A. Siebertz, A. M. Depping, J. Hartmann, F. Hausch, M. V. Schmidt, F. Holsboer, M. Ising, M. B. Cox, U. Schmidt, T. Rein, *Biological psychiatry* **2011**, *70*, 928-936.

[5] a) G. Balsevich, A. S. Hausl, C. W. Meyer, S. Karamihalev, X. Feng, M. L. Pohlmann, C. Dournes, A. Uribe-Marino, S. Santarelli, C. Labermaier, K. Hafner, T. Mao, M. Breitsamer, M. Theodoropoulou, C. Namendorf, M. Uhr, M. Paez-Pereda, G. Winter, F. Hausch, A. Chen, M. H. Tschop, T. Rein, N. C. Gassen, M. V. Schmidt, *Nat Commun* **2017**, *8*, 1725; b) L. A. Stechschulte, B. Qiu, M. Warrier, T. D. Hinds, Jr., M. Zhang, H. Gu, Y. Xu, S. S. Khuder, L. Russo, S. M. Najjar, B. Lecka-Czernik, W. Yong, E. R. Sanchez, *Endocrinology* **2016**, *157*, 3888-3900; c) C. O. Sidibeh, M. J. Pereira, X. M. Abalo, J. B. G, S. Skrtic, P. Lundkvist, P. Katsogiannos, F. Hausch, C. Castillejo-Lopez, J. W. Eriksson, *Endocrine* **2018**, *62*, 116-128.

[6] a) M. Maiaru, O. B. Morgan, T. Mao, M. Breitsamer, H. Bamber, M. Pohlmann, M. V. Schmidt, G. Winter, F. Hausch, S. M. Geranton, *Pain* **2018**, *159*, 1224-1234; b) M. Maiaru, K. K. Tochiki, M. B. Cox, L. V. Annan, C. G. Bell, X. Feng, F. Hausch, S. M. Geranton, *Science translational medicine* **2016**, *8*, 325ra319.

[7] a) S. Gaali, A. Kirschner, S. Cuboni, J. Hartmann, C. Kozany, G. Balsevich, C. Namendorf, P. Fernandez-Vizarra, C. Sippel, A. S. Zannas, R. Draenert, E. B. Binder, O. F. Almeida, G. Ruhter, M. Uhr, M. V. Schmidt, C. Touma, A. Bracher, F. Hausch, *Nat. Chem. Biol.* **2015**, *11*, 33-37; b) S. Gaali, X. Feng, A. Hahle, C. Sippel, A. Bracher, F. Hausch, *J. Med. Chem.* **2016**, *59*, 2410-2422; c) X. Feng, C. Sippel, A. Bracher, F. Hausch, *J. Med. Chem.* **2015**, *58*, 7796-7806.

[8] a) D. M. LeMaster, G. Hernandez, *Current molecular pharmacology* **2015**, *9*, 5-26; b) S. M. Mustafi, D. M. LeMaster, G. Hernandez, *Biochem. J.* **2014**, *461*, 115-123.

[9] D. Shi, Q. Bai, S. Zhou, X. Liu, H. Liu, X. Yao, *Proteins* **2018**, *86*, 43-56.

[10] a) D. M. LeMaster, S. M. Mustafi, M. Brecher, J. Zhang, A. Heroux, H. Li, G. Hernandez, *J. Biol. Chem.* **2015**, *290*, 15746-15757; b) U. Brath, M. Akke, *J. Mol. Biol.* **2009**, *387*, 233-244.

[11] N. A. Farrow, R. Muhandiram, A. U. Singer, S. M. Pascal, C. M. Kay, G. Gish, S. E. Shoelson, T. Pawson, J. D. Forman-Kay, L. E. Kay, *Biochemistry* **1994**, *33*, 5984-6003.

[12] a) J. P. Loria, M. Rance, A. G. Palmer, *J. Am. Chem. Soc.* **1999**, *121*, 2331-2332; b) A. J. Baldwin, L. E. Kay, *Nat. Chem. Biol.* **2009**, *5*, 808-814; c) D. F. Hansen, P. Vallurupalli, L. E. Kay, *Journal of biomolecular NMR* **2008**, *41*, 113-120; d) J. P. Loria, R. B. Berlow, E. D. Watt, *Acc Chem Res* **2008**, *41*, 214-221.

[13] S. Pomplun, C. Sippel, A. Hahle, D. Tay, K. Shima, A. Klages, C. M. Unal, B. Riess, H. T. Toh, G. Hansen, H. S. Yoon, A. Bracher, P. Preiser, J. Rupp, M. Steinert, F. Hausch, *J. Med. Chem.* **2018**, *61*, 3660-3673.

[14] S. Pomplun, Y. Wang, A. Kirschner, C. Kozany, A. Bracher, F. Hausch, *Angewandte Chemie* **2015**, *54*, 345-348.

[15] A. G. Palmer, 3rd, M. J. Grey, C. Wang, *Methods Enzymol.* **2005**, *394*, 430-465.

[16] a) R. Gopalakrishnan, C. Kozany, S. Gaali, C. Kress, B. Hoogeland, A. Bracher, F. Hausch, *J. Med. Chem.* **2012**, *55*, 4114-4122; b) R. Gopalakrishnan, C. Kozany, Y. Wang, S. Schneider, B. Hoogeland, A. Bracher, F. Hausch, *J Med Chem* **2012**, *55*, 4123-4131; c) Y. Wang, A. Kirschner, A. K. Fabian, R. Gopalakrishnan, C. Kress, B. Hoogeland, U. Koch, C. Kozany, A. Bracher, F. Hausch, *J. Med. Chem.* **2013**, *56*, 3922-3935; d) M. Bischoff, C. Sippel, A. Bracher, F. Hausch, *Organic letters* **2014**, *16*, 5254-5257.

[17] O. D. Monera, T. J. Sereda, N. E. Zhou, C. M. Kay, R. S. Hodges, *J Pept Sci* **1995**, *1*, 319-329.

COMMUNICATION

The selective inhibitor SAFit1 uses conformational selection by binding a minor conformation of FKBP51 with an outward conformation of Phe67 in the unbound state.

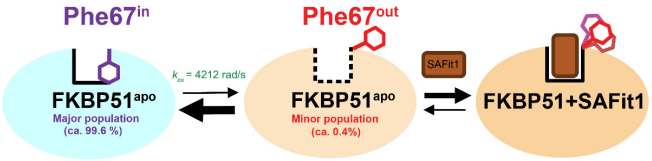

Pravin Kumar Ankush Jagtap, Sam Asami, Claudia Sippel, Ville R. I. Kaila, Felix Hausch, and Michael Sattler

Page No. – Page No.

Selective inhibitors of FKBP51 employ conformational selection of dynamic invisible states

Supplementary Information

Selective inhibitors of FKBP51 employ conformational selection of dynamic invisible states

Pravin Kumar Ankush Jagtap[+], Sam Asami[+], Claudia Sippel, Ville R. I. Kaila, Felix Hausch, and Michael Sattler*

Table of Contents		page
Materials and Methods		S3-S6
Supplementary Discussion		S7
Supplementary References		S7
Table S1	Group fitting of relaxation dispersion data	S8
Table S2	Binding affinity of SAFit1 and FK[431]-16h to FKBP51 and its mutants as determined by SPR	S9
Figure S1	Structures of inhibitors used in this study	S10
Figure S2	^{15}N NMR relaxation data	S11-S12
Figure S3	^{1}H,^{15}N HSQC spectra of the FK1 domains of free and inhibitor bound FBBP51	S13
Figure S4	Representation of internal motion at μs-ms timescales (R_{ex}) based on ^{15}N relaxation dispersion experiments	S14
Figure S5	^{1}H (ΔH) and ^{15}N (ΔN) chemical shift differences	S15
Figure S6	Classical molecular dynamics (MD) simulations and density functional theory (DFT) models of FKBP in apo and ligand-bound states	S16
Figure S7	Ratio of NMR signal intensities in ^{1}H,^{15}N HSQC spectra of FBKP51 wild type and mutants	S17
Figure S8	Superposition of ^{1}H ^{15}N HSQC spectra of FKBP51^{Phe67Tyr} free and in the presence of 1.5-molar FK[431]-16h	S18
Figure S9	Surface Plasmon Resonance experiments	S19
Figure S10	Correlation of equilibrium binding values (K_D) derived from ITC and SPR	S20

Supplementary Methods

Protein expression and purification

The FK1 domain of FKBP51^{WT} (residue 16-140), FKBP51^{Phe67Tyr} and FKBP51^{Phe67Val} was expressed as previously reported[1] in LB for ITC and SPR or M9 media supplemented with either $^{15}NH_4Cl$ for producing ^{15}N labelled protein Or $^{15}NH_4Cl$ and ^{13}C D-glucose for producing ^{13}C, ^{15}N labelled protein. The protein was purified on Ni^{2+} column followed by overnight cleavage of His tag with TEV protease, 2nd Ni^{2+} column to remove the cleaved His tag and a final size exclusion in 10mM potassium phosphate, 100mM NaCl, and 1mM DTT, pH 6.8. Protein was concentrated to 1mM and snap-frozen in liquid nitrogen until further use.

NMR experiments

NMR backbone experiments for FKBP FK1 domain (HNCA, HNCACB and CBCACONH), FKBP+1.5X compound FK[431]-16h (HNCACB and CBCACONH) and FKBP+1.5X SAFit1 (HNCACB and CBCACONH) and transverse relaxation experiments (R_1, R_2, heteronuclear NOE) experiments were recorded at 600 MHz spectrometer at 298 K. For transverse relaxation data peaks were integrated and fit with Pint software[2]. Peaks with severe overlap were omitted from further analysis. For ^{15}N relaxation dispersion experiments, data were recorded at 600 MHz and 900 MHz at 283 K.

NMR relaxation dispersion

The μs-ms dynamics of the amide backbone of FKBP^{WT} in the presence and absence of 1.5X SAFit1 and 1.5X compound FK[431]-16h, respectively, was probed by SQ CPMG relaxation dispersion experiments. Dispersion profiles were obtained at 283 K and external magnetic field strengths of 14.1 T (600 MHz ^1H) and 21.1 T (900 MHz ^1H), respectively. ^1H continuous wave decoupling was employed throughout both constant-time echo periods with a rf ampltiude of 12.5 kHz.[3] The CPMG field ν_{CPMG} was varied from 25 to 1000 Hz, while T_{rel} was set to 40 ms and the pre-scan delay to 2 s. ^{15}N 180° refocusing pulses were applied at ~5.6 kHz. The equilibration delay to achieve equilibrium populations of ground and excited states prior to the CPMG train was set to 5 ms. Amid resonance intensities $I(\nu_{\mathrm{CPMG}})$ were converted to transverse relaxation rates by

$R_{2,\mathrm{eff}}(\nu_{\mathrm{CPMG}}) = -{}^{1}/_{T_{\mathrm{rel}}} \ln {}^{I(\nu_{\mathrm{CPMG}})}/_{I_0}$, where I_0 is the intensity, when omitting the CPMG train. The experimental error was set to two times the standard deviation of the spectral noise.

The fitting procedure is described in the following. Dispersion curves were fitted employing the Carver-Richards equation for a system undergoing chemical exchange in two states, while fitting four independent parameters, namely the exchange rate k_{ex}, the population of the excited state p_a, the absolute chemical shift difference between both states $|\Delta\omega|$, and the transverse relaxation rate in the absence of exchange $R_{2,0}$, assuming equal relaxation rates in both states.[4] For each residue curves at both available fields were fitted simultaneously. To quantitatively discriminate exchanging from non-exchanging residues, all curves were additionally fit by a linear function. The model, which represents the data the best, was selected based on the comparison of AICc (Akaike information criterion, with a correction for small sample size) values.[5] To improve the fitting performance, several residues that are located on the same secondary structure element were grouped together, while employing the χ^2 ratio for group over individiual fitting.[6] Residues with ratios larger than two were discarded, assuming they undergo conformational fluctuations distinct from the global process.

DFT calculations

The structure of apo- and ligand-bound FKBP (PDB ID: 3D5Q and 4TW7) was inserted into a water-ion box with 150 mM NaCl salt concentration. Parameters for the SAFit-ligand were derived from the CHARMM General Force Field (CGenFF) [7], and the remaining of the protein-water-ion system was modelled with the CHARMM36 force field [8]. The systems were simulated for 100 ns, using a 1 fs timestep, T=310 K, and by treating the long-range electrostatics with the particle mesh Ewald (PME) approach. Based on structure extracted from the MD simulations, we constructed quantum chemical cluster models with 56-74 atoms, which were optimized at the B3LYP-D3/def2-SVP level [9], by fixing the position of terminal carbon atoms. Polarization of the protein-water interface were modeled with the conductor-like screening model (COSMO) [10] (7) with a dielectric constant set to e=18. Magnetic shieldings were calculated at the B3LYP-D3/def2-TZVP

level. All classical calculations were performed using NAMD2 [11], and quantum chemical calculations with TURBOMOLE v. 6.6 [12]

ITC experiments

ITC experiments were performed at 25 °C on MicroCal iTC200 instrument with titrating inhibitor in protein. The purified protein was dialyzed overnight against 10mM KPi pH 6.8, 100mM NaCl, 1mM BME and 0.5% DMSO (v/v final concentration) were added to the protein prior to the experiment. Protein concentrations used for different experiments varied from 10-30 μM and corresponding 10-fold inhibitor concentration in the syringe. Data fits were performed with the Microcal Origin software provided with the instrument with a single binding site model. All titrations were performed as duplicates, errors were calculated by error propagation.

Surface plasmon resonance

For SPR experiments, His tag $FKBP^{WT}$ or its mutants were used. The experiments were performed on Biacore X100 system (GE Healthcare). The protein was covalently immobilized on the Biacore sensor chip NTA using His tag mediated capture coupling essentially as described in [13]. Briefly, the flow channel 2 of Biacore sensor chip NTA was regenerated initially by injecting 20 μL of regeneration buffer (10 mM HEPES pH 7.4, 150 mM NaCl, 350 mM EDTA, 0.05% (v/v) NP-40 and after washing the chip with 10 mM HEPES pH 7.4, 150 mM NaCl, 0.05% NP-40, by injecting 40 μL of 500 μM Nickle Sulphate solution. 30 μL of coupling solution (1:1 (v/v) mixture of 100mM N-hydroxysuccinimide (NHS) / 500mM N-ethyl-N-(3-diethylaminopropyl)carbodiimide (EDC)) was injected immediately followed by 1μM His–FKBP51 (in 10 mM HEPES pH 7.4, 150 mM NaCl, 0.05% NP-40) or its mutant at a rate of 5 μL/min till protein immobilization of approximately 2500 RU was achieved on flow channel 2. The EDC/NHS crosslinking was quenched by injecting 35 μL of 1M ethanolamine and the bound Ni^{2+} was further stripped off by injecting 20 μL of regeneration buffer. Similar modification on flow channel 1 was performed but without protein and flow channel 1 was used as a

reference channel. The experiments were carried out in 10 mM potassium phosphate, 100 mM NaCl, 0.05% NP40 and 0.5% DMSO, pH 6.8. Various concentrations of ligands were injected in random order for 180 s at a flow rate of 30 μL/min and the complex was allowed to dissociate in running buffer for another 1200 s. Two concentrations were injected in duplicates along with a buffer blank. Reference channel subtracted data were fit to a simple 1:1 interaction model using global data analysis option available in the BIAEvaluation software provided by the supplier. k_{off} rates for FKBP51^{Phe67Tyr}+FK[431]-16h were very fast due to its very weak affinity and could not be reliably determined as they were outside the limits that could be measured by the instrument.

Supplementary Discussion

ITC and SPR data analysis

In order to assess the thermodynamic and kinetic features of SAFit1 binding to FKBP51 and its mutants, we performed ITC and SPR experiments, respectively, to determine the contributions of enthalpy and k_{on}/k_{off} rates on the binding of inhibitors to wildtype and mutant FKBP5^{WT}. ITC provides information about the enthalpy change associated with ligand binding. However, it does not provide any measure of binding kinetics. SPR provides information about the binding kinetics of molecular interactions.

From ITC measurements, both FKBP51^{WT} mutants, FKBP51^{Phe67Tyr} and FKBP51^{Phe67Val} show a ≈4-fold increase in binding affinity to SAFit1 compared to FKBP51^{WT}. This is accompanied by a ≈4.5 kcal/mol improved binding enthalpy, consistent with the tighter interaction of SAFit1 with the mutant proteins. This is consistent with our NMR data showing that the tyrosine side chain at position 67 in FKBP51^{Phe67Tyr} already preferentially adopts a flipped-out state. The larger binding enthalpy also is consistent with our hypothesis that the energetic penalty for the displacement of Valine at position 67 in FKBP51^{Phe67Val} is relatively minor compared to Phe in FKBP51^{WT}. However, the 4.5-fold kcal/mol increase in binding enthalpy associated with binding of SAFit1 to both mutants is counteracted by a unfavorable entropy compared to FKBP51^{WT} binding (difference in $-T\Delta S$ ≈ 3.9 kcal/mol). Accordingly, the minor overall change in Gibb's free energy yields only a 4-fold increase in binding affinity to SAFit1 for FKBP51^{WT}. This is a classic case of enthalpy-entropy compensation effect observed in protein-ligand interactions[14].

The equilibrium dissociation constants (K_D) obtained from ITC and SPR for the titration of SAFit1 in FKBP51^{WT} and mutants (**Figure S10; Table S2**) are in good agreement. A systematic offset is found for the titration with SAFit1 where SPR-derived K_D values are ~4-fold higher than those obtained by ITC. This may reflect differences in buffer conditions and method, i.e. possibly related to the immobilization of one binding partner in the SPR studies. The correlation of SPR and ITC derived K_D values for the canonical FK[431]-16h inhibitor show a low correlation (**Figure S10; Table S2**).

References

[1] A. Bracher, C. Kozany, A. K. Thost, F. Hausch, *Acta Crystallogr D Biol Crystallogr* **2011**, *67*, 549-559.
[2] A. Ahlner, M. Carlsson, B. H. Jonsson, P. Lundstrom, *J. Biomol. NMR* **2013**, *56*, 191-202.
[3] D. F. Hansen, P. Vallurupalli, L. E. Kay, *The journal of physical chemistry. B* **2008**, *112*, 5898-5904.
[4] a) J. P. Carver, R. E. Richards, *Journal of Magnetic Resonance (1969)* **1972**, *6*, 89-105; b) R. Ishima, D. A. Torchia, *J. Biomol. NMR* **2006**, *34*, 209-219.
[5] a) H. Akaike, *IEEE Transactions on Automatic Control* **1974**, *19*, 716-723; b) E. J. d'Auvergne, P. R. Gooley, *J. Biomol. NMR* **2003**, *25*, 25-39.
[6] F. A. A. Mulder, A. Mittermaier, B. Hon, F. W. Dahlquist, L. E. Kay, *Nat. Struct. Mol. Biol.* **2001**, *8*, 932-935.
[7] K. Vanommeslaeghe, E. Hatcher, C. Acharya, S. Kundu, S. Zhong, J. Shim, E. Darian, O. Guvench, P. Lopes, I. Vorobyov, A. D. Mackerell, Jr., *J Comput Chem* **2010**, *31*, 671-690.
[8] R. B. Best, X. Zhu, J. Shim, P. E. Lopes, J. Mittal, M. Feig, A. D. Mackerell, Jr., *J Chem Theory Comput* **2012**, *8*, 3257-3273.
[9] a) C. Lee, W. Yang, R. G. Parr, *Phys Rev B Condens Matter* **1988**, *37*, 785-789; b) S. Grimme, J. Antony, S. Ehrlich, H. Krieg, *J Chem Phys* **2010**, *132*, 154104; c) F. Weigend, R. Ahlrichs, *Phys Chem Chem Phys* **2005**, *7*, 3297-3305; d) A. D. Becke, *The Journal of Chemical Physics* **1993**, *98*, 5648-5652.
[10] A. Klamt, G. Schuurmann, *Journal of the Chemical Society, Perkin Transactions 2* **1993**, 799-805.
[11] J. C. Phillips, R. Braun, W. Wang, J. Gumbart, E. Tajkhorshid, E. Villa, C. Chipot, R. D. Skeel, L. Kale, K. Schulten, *J Comput Chem* **2005**, *26*, 1781-1802.
[12] R. Ahlrichs, M. Bär, M. Häser, H. Horn, C. Kölmel, *Chemical Physics Letters* **1989**, *162*, 165-169.
[13] A. J. Kimple, R. E. Muller, D. P. Siderovski, F. S. Willard, *Methods Mol Biol* **2010**, *627*, 91-100.
[14] R. Lumry, S. Rajender, *Biopolymers* **1970**, *9*, 1125-1227.

Table S1

Residue	$\lvert\Delta\omega(^{15}N)\rvert$ [ppm]	$R_{2,0}$(14.1 T) [rad/s]	$R_{2,0}$(21.1 T) [rad/s]
Phe67	4.38 ± 0.04	15.2 ± 0.5	19.3 ± 0.5
Asp68	4.59 ± 0.04	16.0 ± 0.4	20.0 ± 0.6
Ser69	5.48 ± 0.03	19.6 ± 0.2	29.6 ± 0.2

Table S1. Group fitting of relaxation dispersion data for residues in strand β3a in unbound FKBP51^{WT}. Globally fitted parameters are: k_{ex} = 4212 ± 48 [rad/s], p_A = 0.9966. All residues on this strand show mobility on the μs-ms timescale (**Figure S4**). Note, that Glu75 in the loop flanking β3a shows overall the largest exchange contribution (**Figure S4**). However, this residue was not further considered for quantitative analysis of the dynamics, as its dispersion appears to be a singularity. The strong exchange contribution to relaxation of this residue is likely induced by dynamic ring current effects induced by dynamics of the aromatic side chain of Phe77, which is in close spatial proximity to the Glu75 amide. Consistent with this Asn74, the residue next to Glu75, shows no dispersion.

To illustrate the significance of these parameters for Phe67 (circles for experimental points), relaxation dispersion curves were plotted, varying the population of the excited state (p_B = 1 - p_A) and the chemical shift difference (Δω):

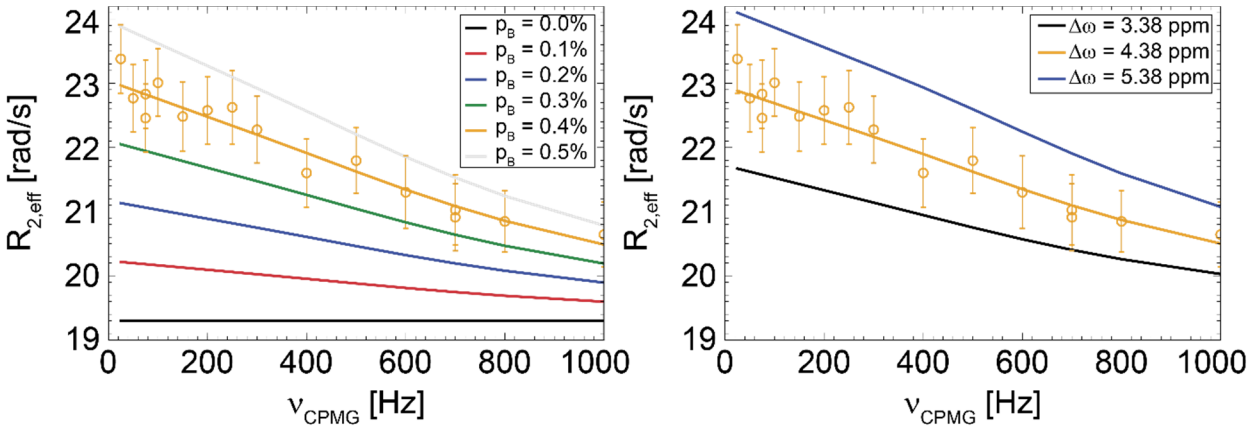

Table S2

Sample	K_D (nM)[a]	K_D (SPR)/K_D(ITC)
FKBP51^{WT}+SAFit1	182 ± 4.7	4.5
FKBP51^{Phe67Tyr}+SAFit1	33.7 ± 2.8	3.6
FKBP51^{Phe67Val}+SAFit1	64.7 ± 1.0	4.4
FKBP51^{WT}+FK[431]-16h	43.9 ± 0.6	0.29
FKBP51^{Phe67Tyr}+FK[431]-16h	N.D.	N.D.
FKBP51^{Phe67Val}+FK[431]-16h	56.8 ± 1.9	0.74
[a] Errors calculated from error propagation of fitting errors. ND: Note defined		

Table S2. Binding affinity of SAFit1 and FK[431]-16h to FKBP51 and its mutants from the kinetic on and off-rates determined by SPR and the ratio of affinities determined by SPR and ITC respectively.

Figure S1

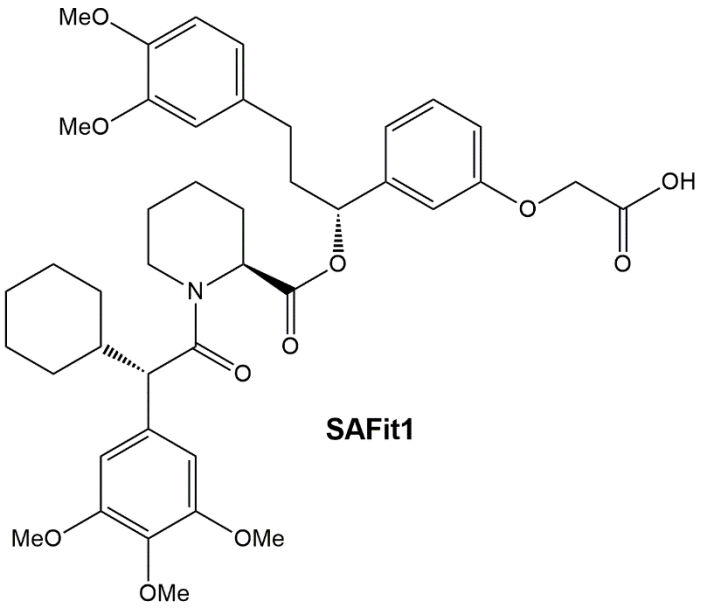

SAFit1

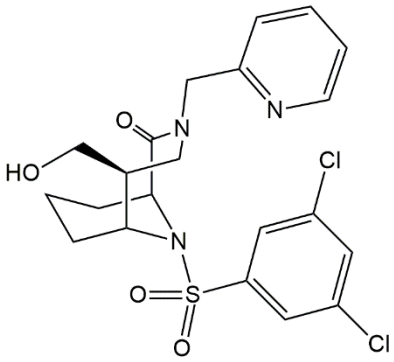

FK[431]-16h

(corresponds to compound 16h from Pomplun et al, J Med Chem 2018, 61, 3660-73)

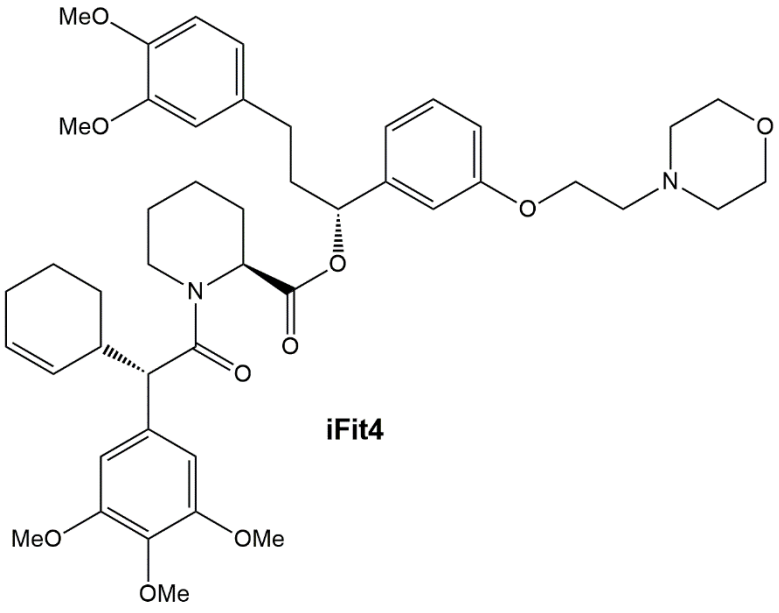

iFit4

Figure S1. Structures of inhibitors used in this study.

Figure S2

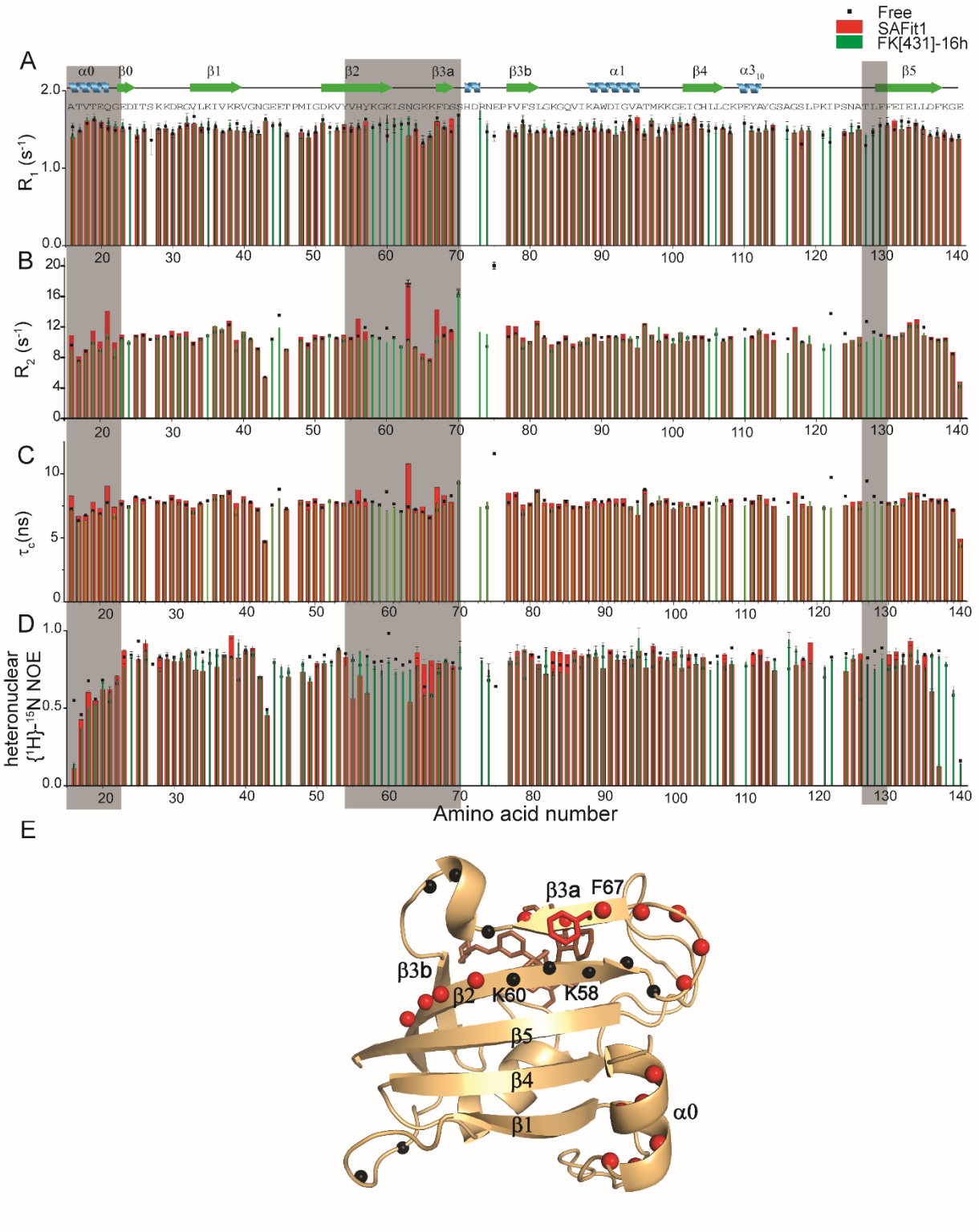

Figure S2. ^{15}N NMR relaxation data. (A) R_1, (B) R_2 (C) τ_c and (D) heteronuclear {^{1}H}-^{15}N NOE for FKBP51^{WT} (black), FKBP51^{WT}+SAFit1 (red) and FKBP51^{WT}+compound FK[431]-16h (green).

Local correlation time (τ_c) derived from ^{15}N NMR relaxation experiments for amides in FKBP51^{WT} (black dots; average τ_c = 7.6 ns), FKBP51+SAFit1 (red bars; average τ_c = 7.8 ns) and FKBP51+ FK[431]-16h (green bars; average τ_c = 7.5 ns). Upon SAFit1 addition, residues Lys58-Ser62 from the β_2 strand are exchange broadened. Upon addition of SAFit1, residues from β_2, β_{3a} sheets and α_0 helix show a significant increase in R_2 relaxation (highlighted by a grey box) signifying the presence of slow exchange in these residues as compared to free and compound FK[431]-16h-bound FKBP51. Besides this, from heteronuclear NOE experiment, residues from the β_2 strand show increased flexibility in the presence of SAFit1 and rigidification in the residues of loop between β_2 and β_{3a} strands. E) Residues, which exhibit increased R_2 relaxation rates upon SAFit1 binding, are plotted as red spheres on the structure of FKBP51 bound to the SAFit1-analog iFit4 (**Figure S1**). Black spheres show residues that were not observed in the ^{1}H-^{15}N HSQC spectrum due to exchange broadening.

Figure S3

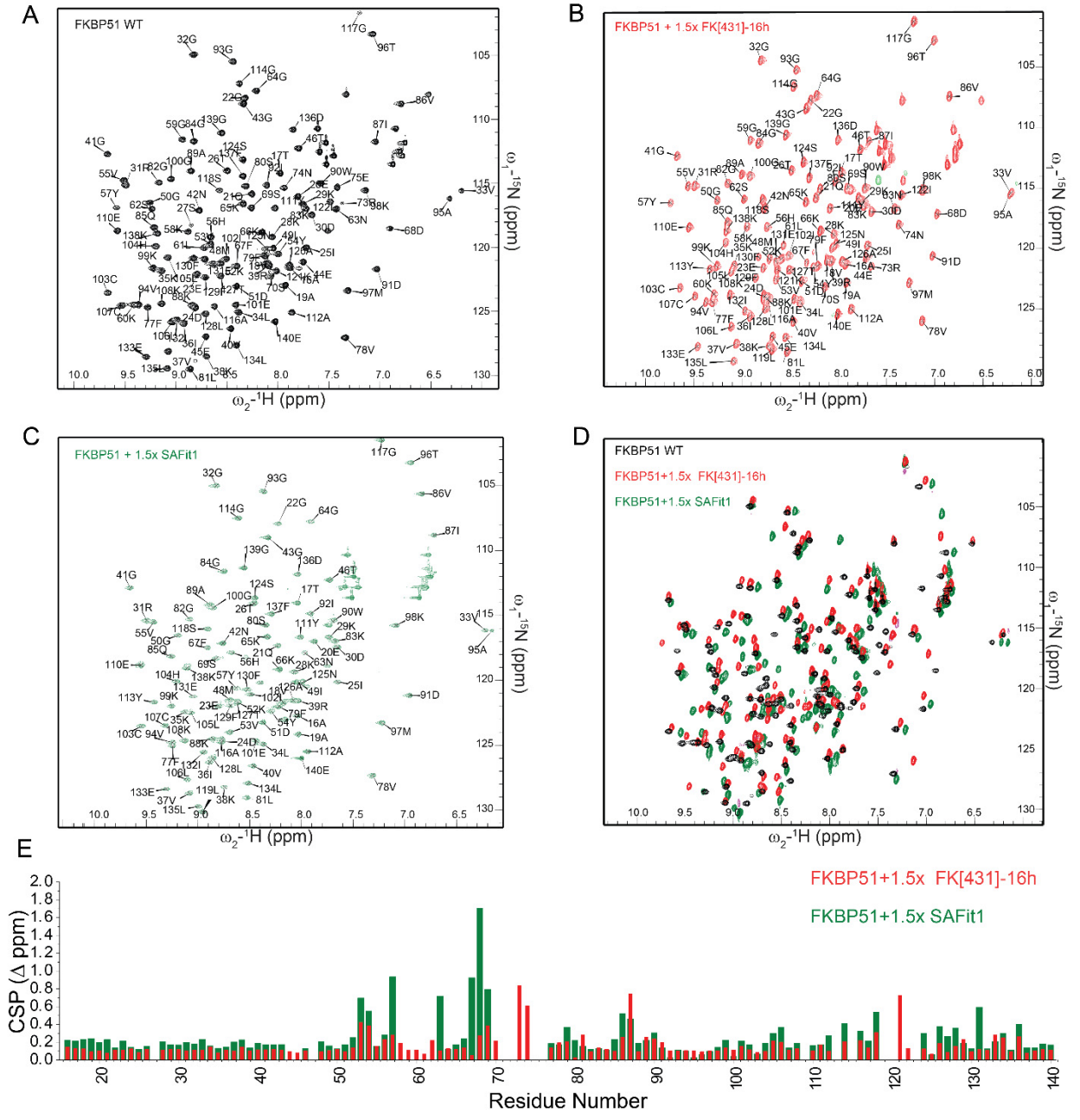

Figure S3. $^{1}H,^{15}N$ HSQC spectra of the FK1 domains of free and inhibitor bound FKBP51. A) Backbone assignments annotated of the FK1 domain of FKBP51 (residues 16-140). Spectra of the FK1 domain B) in presence of 1.5-molar excess of the canonical inhibitor FK[431]-16h, and C) and 1.5-molar excess of SAFit1. D) Superposition of HSQC spectra of FKBP51 free (black) and FKBP51 bound to inhibitors (red, green). E) Chemical shift perturbations plot of FKPB51 upon titration with 1.5x FK[431]-16h (red) or 1.5x SAFit1 (green).

Figure S4

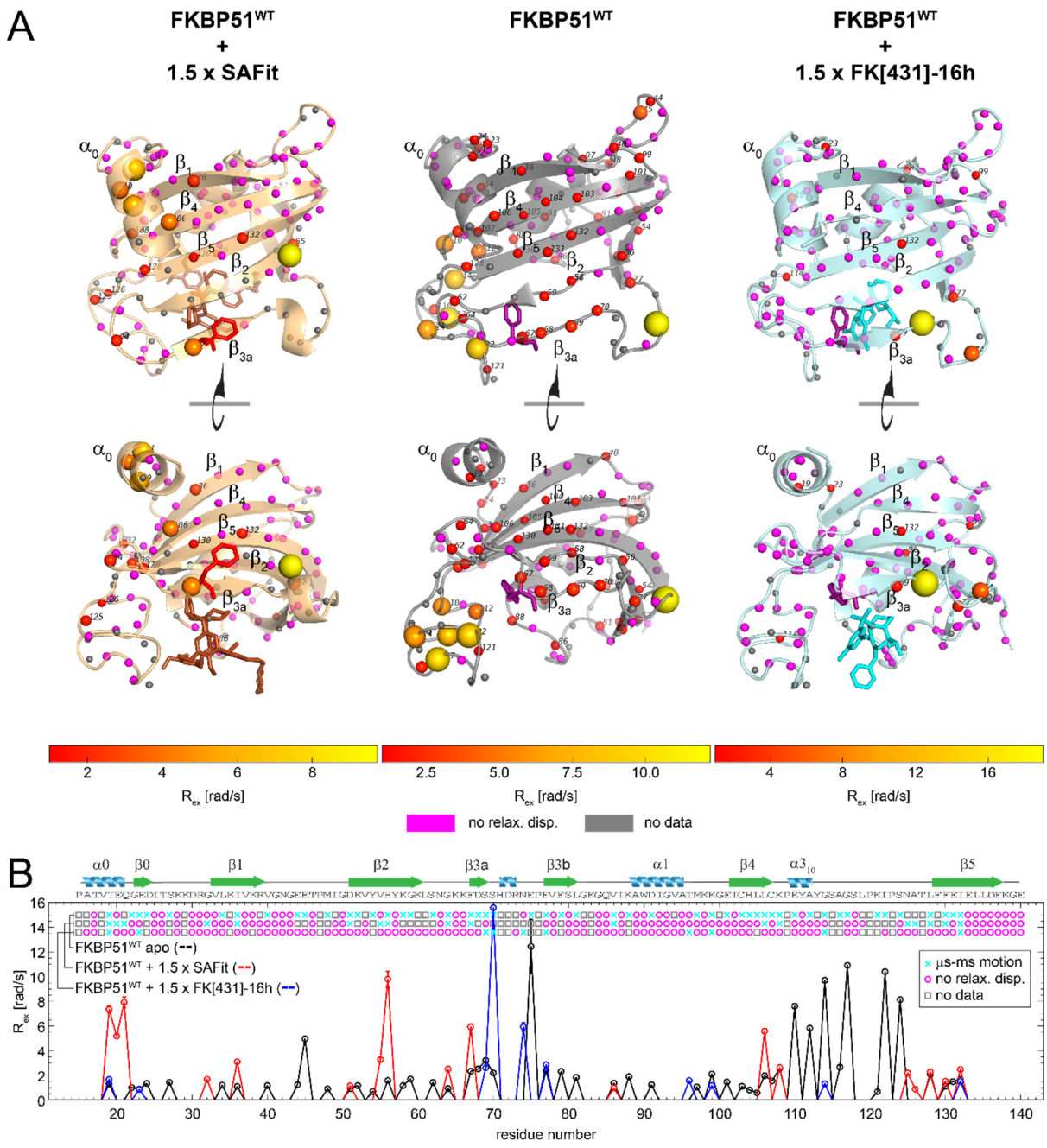

Figure S4. Representation of internal motion at µs-ms timescales (R_{ex}) based on ^{15}N CPMG relaxation dispersion experiments recorded for FKBP51^{WT}, FKBP51^{WT}+SAFit1 and FKBP51^{WT}+ FK[431]-16h. A) The exchange rates experienced by different amides are graphically indicated as colored spheres on the structures, cyan and magenta for presence and absence of relaxation dispersion, gray indicates missing data. B) R_{ex} vs. residue measured at B_0 = 21.1 T, T = 283 K at sample concentrations of 1 mM.

Figure S5

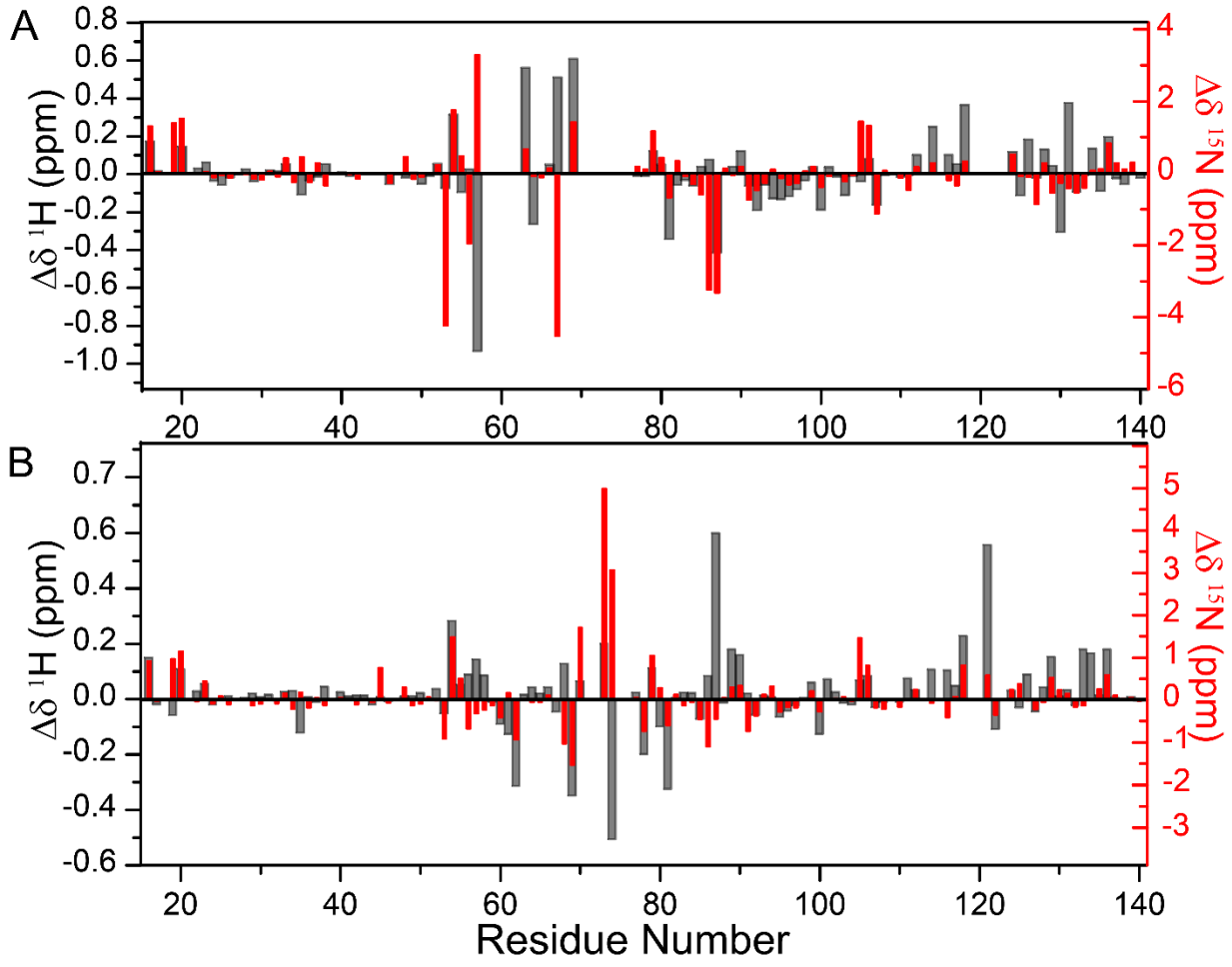

Figure S5. ^{1}H ($\Delta\delta^{1}$H) and ^{15}N ($\Delta\delta^{15}$N) chemical shift differences for NMR spectra recorded at 283K for A) $\Delta\delta$ {FKBP51^{WT} – (FKBP51^{WT} + 1.5x SAFit1)} and B) $\Delta\delta$ {FKBP51^{WT} – (FKBP51^{WT}+ 1.5x FK[431]-16h)}.

Figure S6

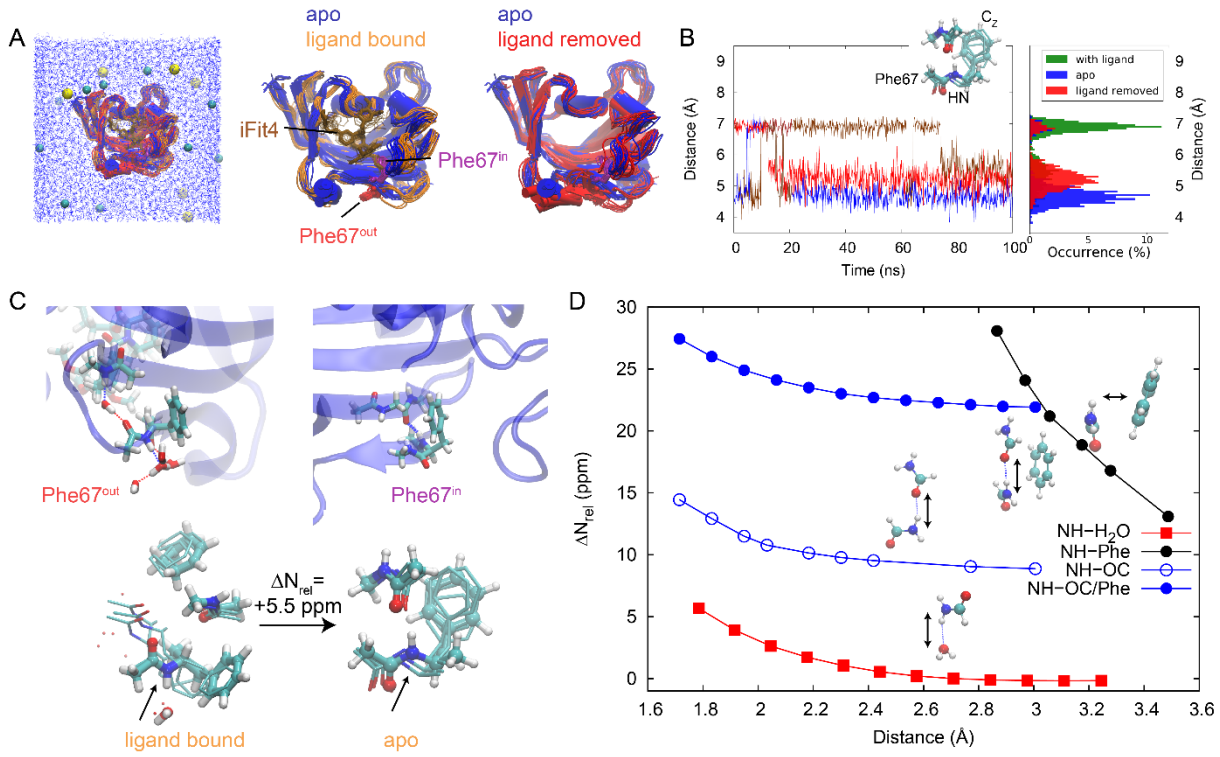

Figure S6. Molecular dynamics (MD) simulations and density functional theory (DFT) models of FKBP51^{WT} in apo and ligand-bound states. A) 100 ns MD simulations of FKBP51^{WT} in the *apo*-state (blue), with the iFit4 ligand (brown), and after removal of iFit4 (red). Phe67 is shown in its inward (Phe67^{in}) and outward (Phe67^{out}) conformations. B) Conformational dynamics of the Phe67 in the apo- and ligand-bound states, and after ligand removal. Fluctuation of distances between the backbone amide (NH) and the aromatic side chain C_z atom of the Phe67 residue during the MD simulation, along with their percentage occurrence in ligand-bound, apo and ligand-removed states are shown. Removal of the ligand leads to an increased sampling of short N-H/aromatic ring distances. C) MD snapshots and optimized DFT models of the ligand-bound and apo-conformations, with the Phe67 N-H forming contacts with bulk water and with the protein peptide bond/the Phe-aromatic ring, respectively. This leads to an average +5.5 ppm ^{15}N chemical shift increase of the Phe67 backbone nitrogen at the B3LYP-D3/def2-TZVP level. The standard deviation of 10 optimized DFT-structures selected from the 100 ns MD trajectory was +1.7 ppm. D) Gas-phase DFT models (B3LYP-D3/def2-TVZP) tested on a small model system in vacuum showing how relative N-H chemical shifts are affected by interaction with a water molecule, peptide bond, and an aromatic interaction. Qualitatively, these calculations support the interpretation above. However, due to the small system and vacuum calculations all effects are larger than they would be with full environment screening.

Figure S7

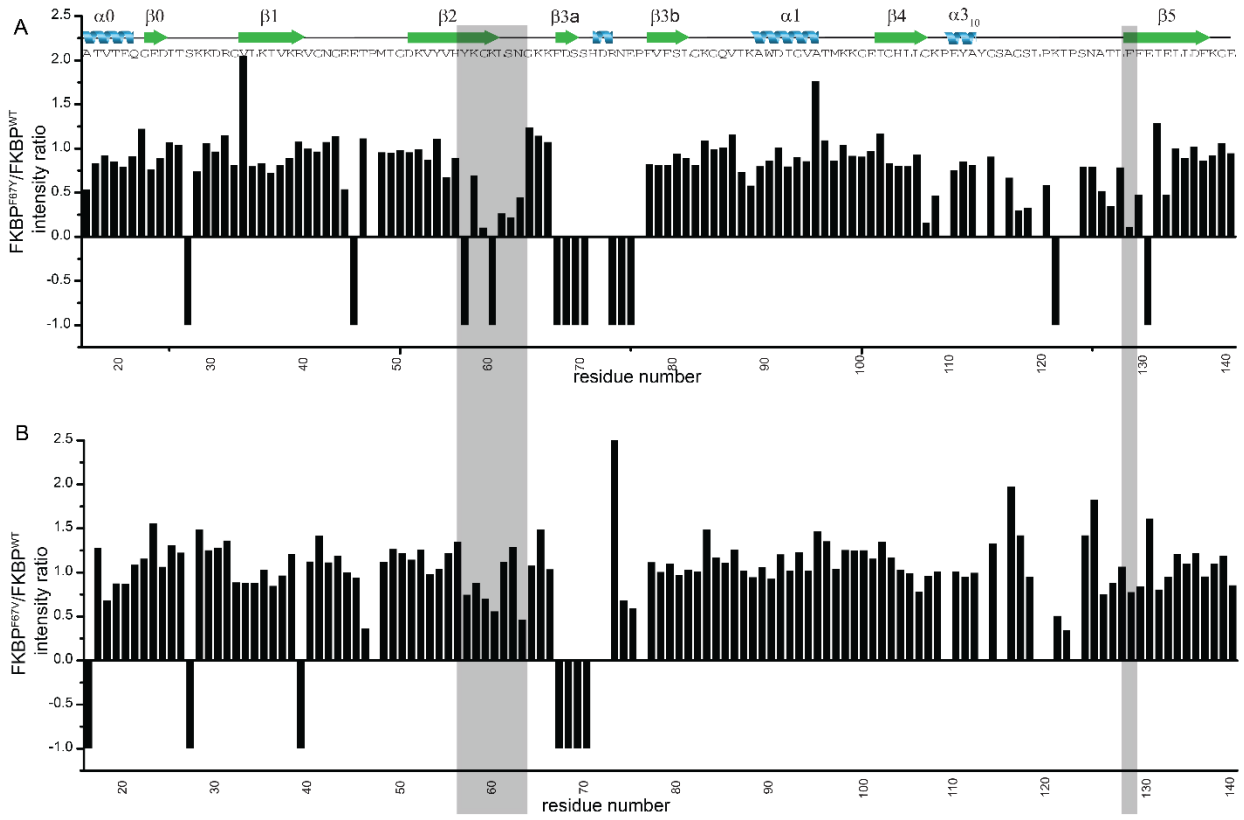

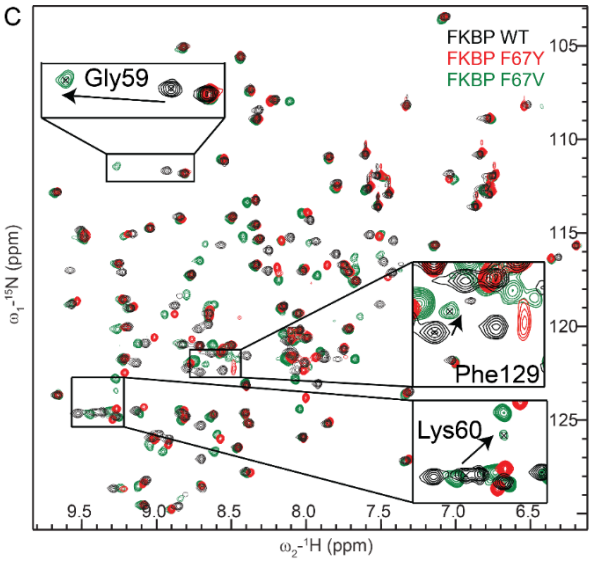

Figure S7. Spectral changes in $^{1}H,^{15}N$ HSQC spectra of FBKP51 wild type and mutants. A) $FKBP51^{Phe67Tyr}$ vs. $FKBP51^{WT}$, B) $FKBP51^{Phe67Val}$ vs. $FKBP51^{WT}$. $FKBP51^{Phe67Tyr}$ shows severe line broadening at the tip of strand β_2 (Gly59, Lys60) and in strand β_5 strand (Phe129), that resemble those observed with FKBP51+SAFit1. This indicates that Tyr67 adopts a flipped out conformation. The line broadening in $FKBP51^{Phe67Val}$ is relatively minor. Residues where NMR signals are not visible in the spectra of mutants are shown as negative bars. C) Superposition of ^{1}H-^{15}N HSQC spectra of $FKBP51^{WT}$, $FKBP51^{Phe67Tyr}$ and $FKBP51^{Phe67Val}$.

Figure S8

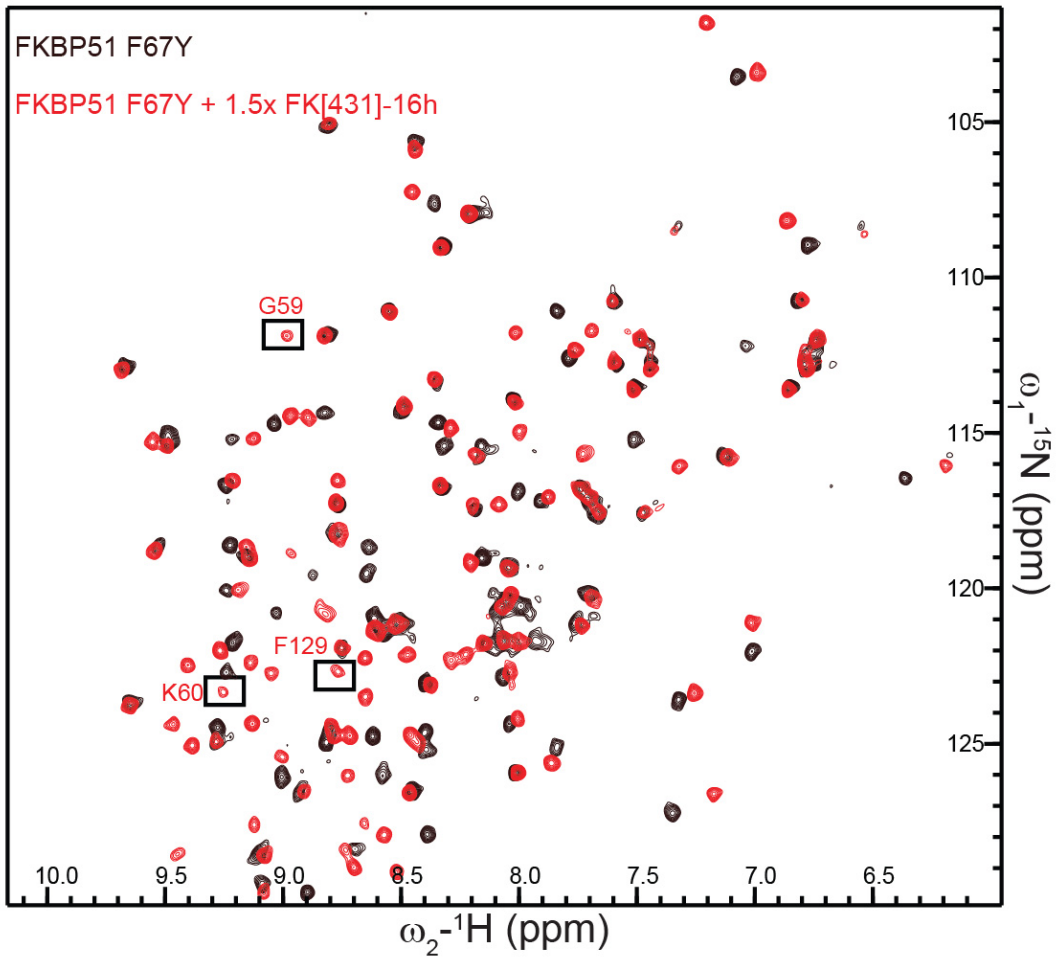

Figure S8. Superposition of ^{1}H ^{15}N HSQC spectra of FKBP51^{Phe67Tyr} free and in the presence of 1.5-molar excess of FK[431]-16h. Spectra of the FKBP51^{Phe67Tyr} mutant exhibit severe line broadening at the tip of β_2 strand resembling FKBP51^{WT}+SAFit1. If Tyr67 is stabilized in the flipped-in conformation in the presence of the ligand, a reduction of dynamics and thus line-broadening is expected. Tyr67 is likely stabilized in a flipped-in conformation and contributes to the binding pocket for FK[431]-16h. This is indeed observed for FKBP^{Phe67Tyr} in the presence of 1.5-molar FK[431]-16h, where signals for residues Gly59 and Lys60 present at the tip of β_2 strand are now observable.

Figure S9

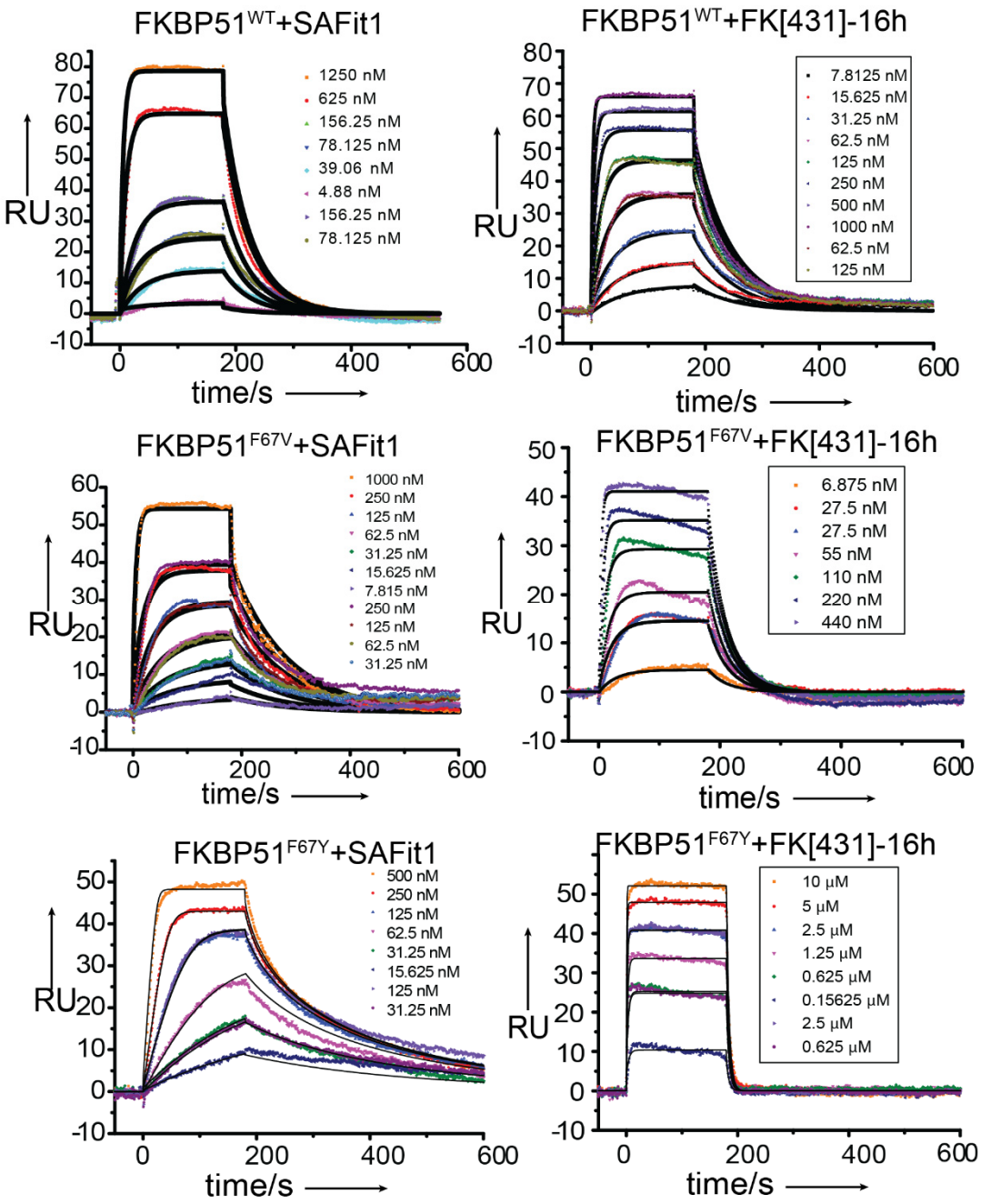

Figure S9. Surface Plasmon Resonance experiments of FKBP51 wild type and mutants with different ligands.

Figure S10

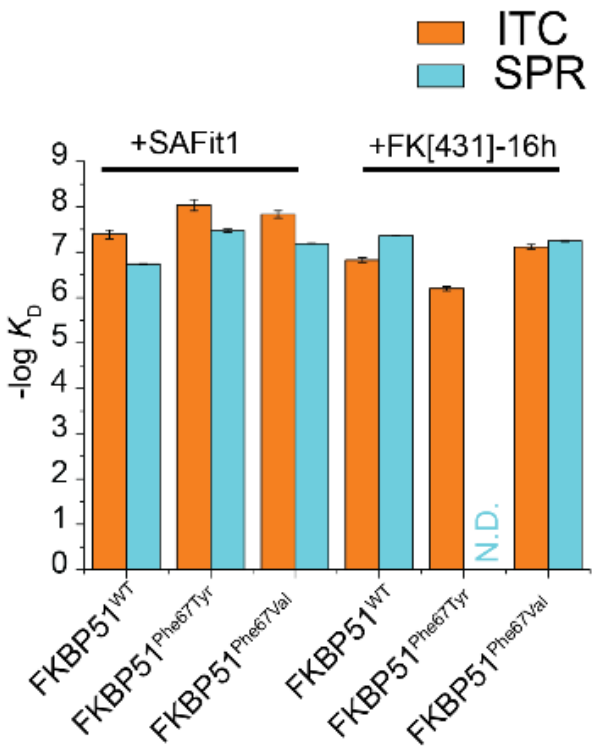

Figure S10. Correlation of equilibrium binding values (K_D) derived from ITC and SPR. Dissociation constants (K_D) derived from ITC (orange) and SPR (light blue) for SAFit1 show an ~4-fold higher affinity compared to ITC values.